Chemical Science

ROYAL SOCIETY OF CHEMISTRY

EDGE ARTICLE

View Article Online
View Journal | View Issue

Cite this: *Chem. Sci.*, 2025, **16**, 12493

All publication charges for this article have been paid for by the Royal Society of Chemistry

Self-supplying coreactant radical and structural distortion induced by carbonate ligand in metal–organic framework for anomalous deep-red Self-electrochemiluminescence†

Lu Zhao,[a] Zhenjie Xu,[a] Xianzhen Song,*[a] Caifeng Ding *[a] and Huangxian Ju *[b]

Received 28th March 2025
Accepted 1st June 2025

DOI: 10.1039/d5sc02359a

rsc.li/chemical-science

Self-electrochemiluminescence (self-ECL) can deal with the problems of limited electron transport efficiency, reduced signal stability, and redundant ECL processes. A feasible solution is to assemble the luminescent components and coreactant radicals together. Here a self-ECL material was designed relying on a europium-based metal–organic framework (Eu-MOF, ZL-2) with 1,10-phenanthroline and CO_3^{2-} as ligands under strong alkaline conditions. Upon oxidation of the CO_3^{2-} ligand to produce $C_2O_6^{2-}$, $OH^{\bullet}$ could be generated to act as a coreactant radical, which reacted with the luminophore radical of oxidized ZL-2 to realize self-ECL without an extra coreactant. The coordination of the CO_3^{2-} ligand induced Eu^{3+} to occupy some sites in the tetrakaidecahedron structure of ZL-2, which caused the structure to distort, and thus triggered the unusual electric-dipole transfer transition $^5D_0$–$^7F_4$. Therefore, ZL-2 was endowed with deep-red luminescence in the first near-infrared (NIR-I) region, which filled a gap in self-NIR-ECL applications. This discovery suggested a novel promising dual-function mechanism of the CO_3^{2-} ligand, undoubtedly broadening the application and development of MOFs in the ECL field.

Introduction

In light of its low background, wide dynamic range and simple operation, electrochemiluminescence (ECL) has emerged as a pivotal technology for clinical diagnosis, drug screening, food and environmental detection, and has been universally acknowledged.[1–3] In particular, ECL emission in the deep-red area displays superior optical penetration, less photodamage, and lower optical scattering,[4] leading to important applications in detection, sensing, optical communication, night vision and other fields.[4–6] The luminophore, which generates high-energy species through redox reactions to realize ECL emission, is regarded as a decisive factor in ECL efficiency. However, in most cases, its high ECL performance is only achieved with the assistance of coreactants. The reaction between two phases reduces electron transport efficiency, which lowers the ECL signal and causes the stability to deteriorate. Moreover, the excessive use of coreactants not only causes redundancy in the design of the ECL process but also generates toxic by-products.[7,8] Therefore, the development of novel ECL materials integrating luminophore and coreactant is essential to broaden the application of ECL technology.[9,10]

MOFs have the characteristics of large active specific surface area, self-assembly properties, *etc.*,[11–13] which can satisfy the demand for the independent design of a high-efficiency luminophore. To integrate the luminophore and coreactant in MOFs for self-ECL, Lei *et al.* used 9,10-di(*p*-carboxyphenyl)-anthracene (DPA) and 1,4-diazabicyclo[2.2.2]octane (D-H_2) as ligands and Zn^{2+} as a bridge to prepare an m-MOF.[7] The presence of DPA as luminophore and D-H_2 as coreactant resulted in a self-ECL function for the m-MOF. They further used *N*,*N*-diethylenediamine (DEDA) as coreactant to synthesize a covalent organic framework (COF) luminophore for self-ECL, which exhibited an extraordinary 1008-fold signal compared with the ECL system of COF and external coreactant DEDA.[14] These results indicate that the self-assembly of coreactants into the framework can greatly shorten the distance between the luminophore and the generated coreactant radical to accelerate the reaction rate, effectively improving the ECL efficiency of framework materials.

Coreactant radicals like $OH^{\bullet}$ and $SO_4^{\bullet-}$ can be generated by a functional ligand with carboxyl or sulfhydryl. Moreover, the oxidation of carbonate (CO_3^{2-}) can also generate $OH^{\bullet}$ through the mediation of peroxydicarbonate ($C_2O_6^{2-}$).[15] Under strong

[a]*Key Laboratory of Optic-Electric Sensing and Analytical Chemistry for Life Science, College of Chemistry and Molecular Engineering, Qingdao University of Science and Technology, Qingdao 266042, P. R. China. E-mail: songxianzhen@qust.edu.cn; dingcaifeng@qust.edu.cn*

[b]*State Key Laboratory of Analytical Chemistry for Life Science, School of Chemistry and Chemical Engineering, Nanjing University, Nanjing 210023, P. R. China. E-mail: hxju@nju.edu.cn*

† Electronic supplementary information (ESI) available: X-ray crystallographic files (CIF), chemicals and apparatus, Experimental procedures, Tables S1, S2 and Fig. S1–S9. CCDC 2427309. For ESI and crystallographic data in CIF or other electronic format see DOI: https://doi.org/10.1039/d5sc02359a

alkaline conditions, CO_3^{2-} can be produced through the decarboxylation of amino acids to provide multiple binding sites for the coordination of the metal ion as a bridge in the structure of MOFs.[16] In view of the eminent ECL performance of lanthanide metal–organic frameworks (Ln-MOFs), the innate advantages of rich ladderlike electronic levels and 4f–4f transitions in Ln-MOFs, which endow them with high luminescent efficiency and long lifetime.[13,17,18] This work has designed a Eu-MOF (ZL-2) as a self-ECL emitter using glycine (Gly) to provide CO_3^{2-} ligand for the generation of coreactant radical $OH^{\bullet}$ and 1,10-phenanthroline (Phen) as the first ligand to increase the structural stability. Surprisingly, ZL-2 showed a rare deep-red self-ECL due to the characteristic luminescence of $^5D_0$–$^7F_4$ transition emission for Eu^{3+} and the self-production of $OH^{\bullet}$. Fluorescence measurements and theoretical calculation demonstrated that the CO_3^{2-} ligand twisted the tetrakaidecahedron structure to form a distorted antiprism structure, which resulted in the electric-dipole $^5D_0$–$^7F_4$ transition with the strongest luminescence intensity. Therefore, ZL-2 demonstrates the prospects of the CO_3^{2-} ligand in the ECL field, and could broaden the ECL application of MOF materials in clinical and environmental detection.

Results and discussion

Single crystal structural analysis of ZL-2

Single-crystal X-ray diffraction analysis showed crystallization of ZL-2 in the space group *C*12/*c*1 (Table S1†) *via* approximately two-fold of the asymmetric unit. The winglike asymmetric unit contained one Eu(III) ion, two coordinated Phen ligands, two coordinated CO_3^{2-} ligands and one coordinated water molecule (Fig. 1A). The nine-coordinated Eu(III) ions were occupied by five O atoms and four N atoms to form a $[Eu_2(CO_3)_2(H_2O)_2]$ cluster with distorted tetrakaidecahedron coordination geometry (Fig. 1B and C), which contained a CO_3^{2-} bidentate ligand in the coordination. Five O atoms coordinated to one Eu(III) ion from one chelated η^2-CO_3^{2-} ligand [Eu1–O1 = 2.395(3) Å and Eu1–O2 = 2.361(2) Å], one bridged μ_2-η2-CO_3^{2-} ligand [Eu1–O4 = 2.4375(6) Å and Eu1–O5 = 2.448(2) Å] and one water molecule [Eu1–O13 = 2.439(2) Å]. Four N atoms were from two chelating η^2-Phen ligands and coordinated to one Eu(III) ion [Eu1–N1 = 2.602(3) Å, Eu1–N2 = 2.576(3) Å, Eu1–N3 = 2.576(3) Å and Eu1–N4 = 2.591(3) Å]. The infinite 2D parallelogram network structure of $[Eu_2(CO_3)_2(H_2O)_2]$, SBUs were cross-connected to each other to form a 3D framework by μ_2-η^2-CO_3^{2-} ligands and abundant H_2O molecules (Fig. 1C and D). The π–π stacking interactions resulting from the intersection of the coordinated Phen group and the neighbouring $[Eu_2(CO_3)_2(H_2O)_2]$ SBUs stabilized the adjacent intersecting frameworks (Fig. 1D). In the whole ZL-2, the O–Eu–O, O–Eu–N and N-Eu–N bond angles were in the ranges of 53.75(8)–150.12(6)°, 70.17(9)°–152.08(9)° and 62.41(8)–152.90(9)°, respectively. The coordinated O–C–O bond angles were 115.3(3)° and 118.3(2)°. To sum up, the bond lengths and angles of ZL-2 were in the normal ranges (Table S2†). The XRD patterns of ZL-2 and ZL-2S are exhibited in Fig. S1.†

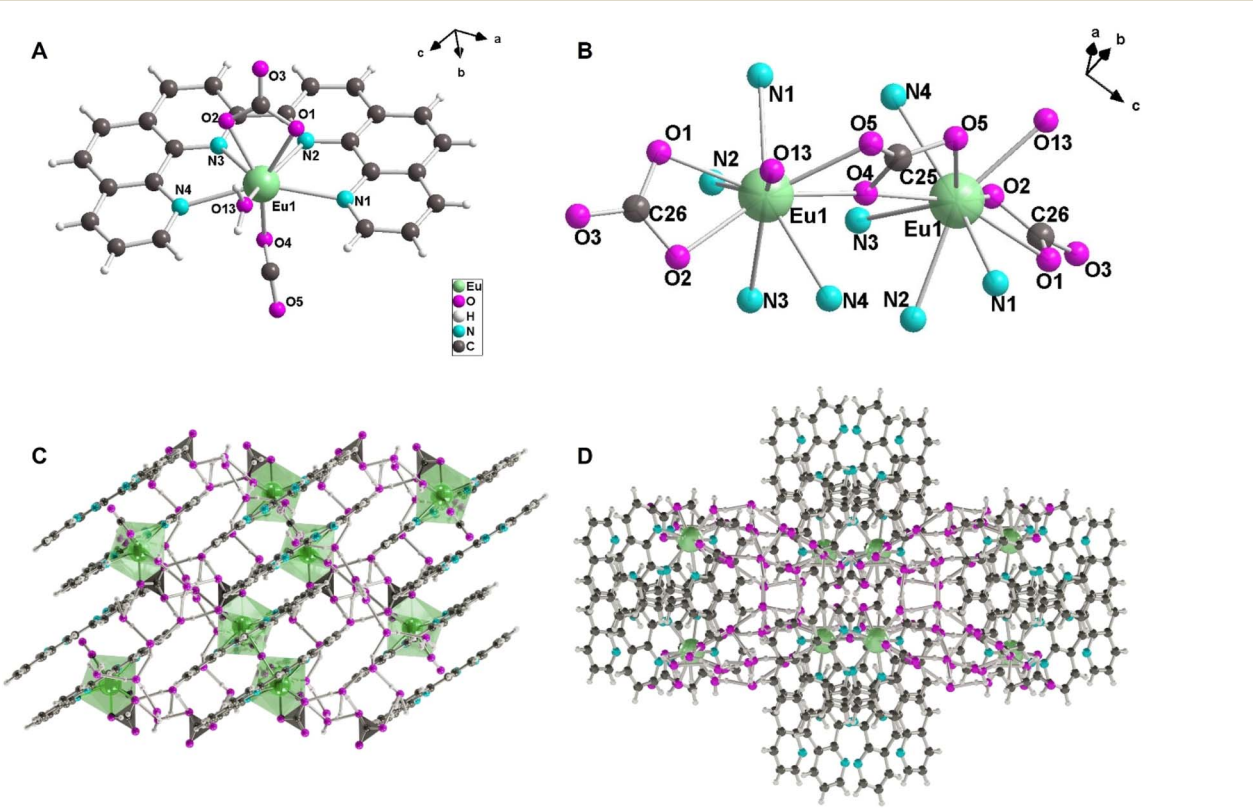

Fig. 1 (A) Coordination environment of Eu(III) ions in ZL-2 (symmetry codes: #1 − *x*, *y*, 3/2 − *z*). (B) Coordination polyhedral geometry of Eu(III) ions. (C) The layer structure with multiple coordination units. (D) Stick model representation of a single 3D framework. Atom color scheme: C, dark grey; N, light blue; O, rosy; H, white; Eu, green.

Self-ECL mechanism of ZL-2

The self-ECL property of ZL-2 in PBS was first investigated with ECL–potential curves. Neither Eu^{3+}-modified nor CO_3^{2-}-modified GCEs showed any ECL response in the potential range of +0.4 to +1.8 V, while Phen-modified GCEs showed weak ECL emission peaking at about +0.9 V (Fig. S2†), which should be attributed to the oxidation of Phen to produce the excited species. In contrast, ZL-2-modified GCE showed a high ECL intensity of 6784 a.u. at +1.72 V in 0.1 M pH 6.38 PBS. Moreover, the ECL intensity depended on solution pH, and the highest ECL intensity occurred at pH 6.38 (Fig. 2A). This variation was unexpectedly consistent with the distribution score curve of carbonic acid. Therefore, the self-ECL behavior of ZL-2 was to some extent related to the CO_3^{2-} ligand in its structure. To confirm this speculation, a single-ligand Eu-MOF without CO_3^{2-} (ZL-2S) was synthesized for comparison of the ECL performance. Unlike ZL-2-modified GCE, ZL-2S-modified GCE showed only a very weak ECL peak at +1.28 V (Fig. 2B), similar to the ECL peak of Phen-modified GCE (Fig. S2†). The more positive ECL peak potential than free Phen-modified GCE could be attributed to coordination between Phen and metal ion Eu(III) to form a new luminous component in single-ligand Eu-MOF. Moreover, the self-ECL signals of ZL-2S under different pH conditions were not significantly different and were all of very low intensity, approximately 480 a.u. (Fig. S3†). Therefore, the much stronger ECL emission of ZL-2-modified GCE at +1.72 V further demonstrated the importance of the CO_3^{2-} ligand in the self-ECL process.

In the anodic process, ZL-2-modified GCE showed an oxidation peak at +1.56 V (Fig. S4†), consistent with the reported potential of the maximum degree of transformation from CO_3^{2-} to HCO_3^- linked to the production of $CO_3^{\bullet-}$ and $C_2O_6^{2-}$.[15,19] Thus, the ECL process included the oxidation of the CO_3^{2-} ligand to produce peroxydicarbonate $C_2O_6^{2-}$, which could then react with H_2O to produce hydrogen peroxide (H_2O_2).[15,20] Subsequently, the redox process of ZL-2-modified GCE for the generation of H_2O_2 was studied using rotating ring-disk electrode measurement.[20] The produced H_2O_2 could be detected by the Pt ring electrode, which exhibited a modest onset potential of +0.38 V with a ring collection efficiency of 37% (Fig. 2C). According to calculation,[21] the H_2O_2 selectivity was 50.13% under the $2e^-$ ORR process with the electron transfer number (n) approaching 2.7 (Fig. 2C and S5†). These results reflected the generation of H_2O_2 in the process of converting CO_3^{2-} into $C_2O_6^{2-}$. Upon the production of H_2O_2, the $OH^\bullet$ radical was activated.[19,22–24] An electron paramagnetic resonance experiment with DMPO as a radical scavenger demonstrated the production of $CO_3^{\bullet-}$, accompanied by the obvious formation of $OH^\bullet$ (Fig. 2D), confirming the occurrence of oxidization of CO_3^{2-} into $C_2O_6^{2-}$ and the production of H_2O_2 in turn. Furthermore, the ECL transients test with different stepping pulses confirmed the function of $OH^\bullet$ (Fig. 2E). At the initial stepping potential of 0 V, the ECL transient of ZL-2 was not observed until the potential was stepped to +1.2 V, at which the oxidation of CO_3^{2-} took place (Fig. S4†), and $OH^\bullet$ was also generated. Afterward, the strongest degree of oxidation was reached at +1.56 V, while the ECL transient intensity of ZL-2 was 3420 a.u. Powered by the whole oxidation up to the potential of +1.8 V, the accumulation of $OH^\bullet$ reached its maximum, leading to the highest ECL transient with a stable intensity of 6784 a.u. In addition, the ECL transient intensity of ZL-2S-modified GCE in PBS containing free CO_3^{2-} showed a similar growth trend

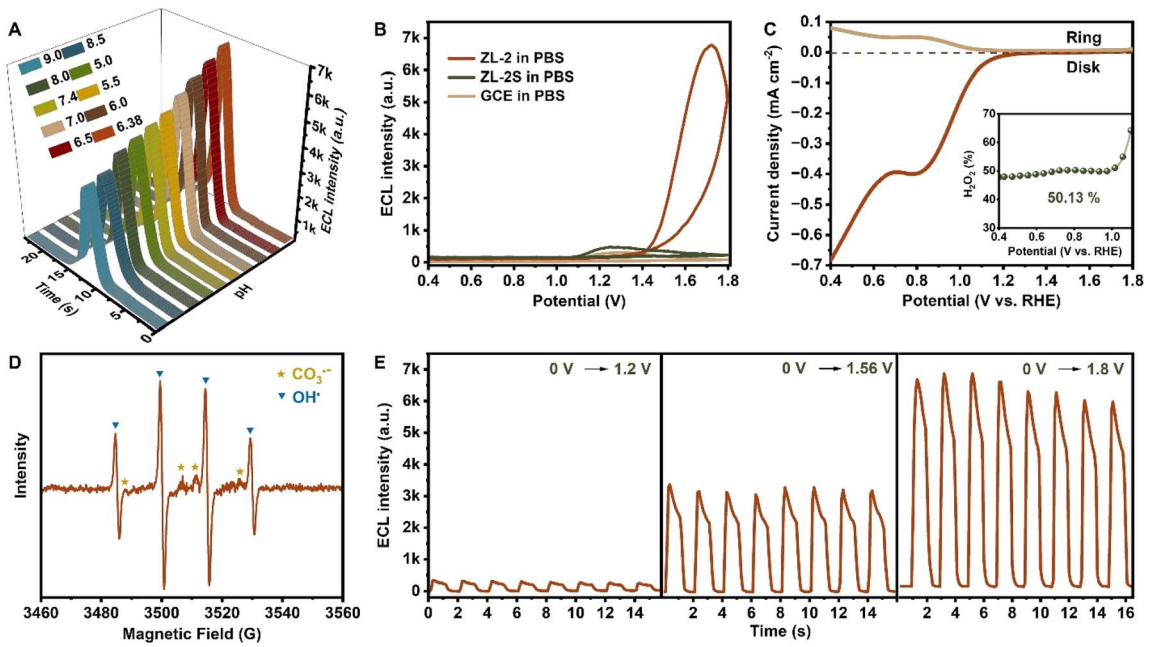

Fig. 2 (A) ECL–time curves of ZL-2-modified GCE in 0.1 M PBS at different pH. (B) ECL–potential curves of ZL-2-modified and ZL-2S-modified GCEs in 0.1 M PBS (pH 6.38). (C) Current–potential curves of rotating-ring-ZL-2-modified disk electrode at 1600 rpm in 0.1 M PBS (pH 6.38). Inset: the selectivity for H_2O_2 production at ZL-2-modified disk electrode. (D) EPR spectrum of ZL-2 in DMPO dispersion for $CO_3^{\bullet-}$ and $OH^\bullet$. (E) ECL transients of ZL-2-modified GCE with steps from 0 V to 1.2, 1.56 and 1.8 V in 0.1 M pH 6.38 PBS.

with a lower signal value (Fig. S6†). Conversely, the ECL transient intensity of ZL-2S-modified GCE in PBS was maintained at the low value of 480 a.u. with increasing stepping potential (Fig. S7†). Therefore, these results indicated that the CO_3^{2-} ligand had a coreactant effect. The generated OH˙ prompted the self-ECL of ZL-2, thanks to the source of the CO_3^{2-} ligand.

To further explore the self-ECL mechanism, the luminous component was confirmed. As mentioned earlier, the ECL curve of Phen-modified GCEs showed a weak ECL peak at +0.9 V, while the ECL peaks of ZL-2-modified and ZL-2S-modified electrodes occurred at +1.72 and +1.28 V (Fig. S2† and 2B), indicating that the luminous component of as-synthesized framework ZL-2 was not the Phen ligand. Although the UV-vis spectra of both ZL-2 and ZL-2S exhibited the characteristic absorption peaks belonging to the Phen ligand, the existence of the second ligand CO_3^{2-} resulted in a red shift and extended the absorption band (Fig. S8†), revealing improved coordination stability.[25] Thus the CO_3^{2-} ligand changed the structure of the MOF.

The fluorescence spectra of ZL-2 showed excitation bands at 350 and 387 nm (Fig. 3A), which were matched with the $^7F_0$–$^5D_4$ and $^7F_0$–$^5L_7$ transitions of Eu^{3+}, and the emission bands centered at 594, 618, 653 and 705 nm were ascribed to $^5D_0$–$^7F_1$, $^5D_0$–$^7F_2$, $^5D_0$–$^7F_3$ and $^5D_0$–$^7F_4$ transitions of Eu^{3+}.[5,26] These phenomena reflected the antenna effect in ZL-2 that was the energy transfer process from the Phen ligand to Eu^{3+}. Electron DFT calculation and natural transition orbital (NTO) analysis were used to theoretically verify the antenna effect in ZL-2. As shown in Fig. 3B, the transition from the ground state (S_0) to the excited singlet state (S_1) was concentrated in $[Eu_2(CO_3)_2(H_2O)_2]$ SBUs, and the transition of NTO 276 to 277 was the dominant proportion (67.44%). In terms of the changes in electron cloud and fluorescence spectra, it could be concluded that the luminescence center in ZL-2 was the Eu unit. The energy gap ($E_{S_1} - E_{T_1}$) of 2038.97 cm^{-1} between S_1 and the triplet first excited state (T_1) of the Phen ligand as well as the energy difference of 5496.65 cm^{-1} between T_1 of Phen and the excited state of Eu^{3+} ($E_{T_1} - E_{Eu^{3+}}$) met the occurrence criteria of the antenna effect.[27] Thus the antenna effect could be described in a schematic diagram (Fig. 3C). These results confirmed that the self-ECL mechanism of ZL-2 was accomplished through the Eu unit as the luminophore and the CO_3^{2-} ligand as the coreactant. The oxidation of CO_3^{2-} produced $CO_3^{\bullet-}$ to form $C_2O_6^{2-}$ and then reacted with water to produce H_2O_2 followed by OH˙.[15,24] The OH˙ radical reacted with the electro-oxidized product of ZL-2 (ZL-2$^{\bullet+}$ radical) to generate excited ZL-2*, accompanied by energy transfer from the Phen ligand to the central Eu unit, thus achieving self-ECL. Moreover, the process of CO_3^{2-} oxidation to induce the formation of OH˙ created a cycle to supply CO_3^{2-} continuously, maintaining the steady ECL signal. The self-ECL mechanism diagram of ZL-2 is shown in Fig. 3D.

Ligand-induced deep-red emission of self-ECL

In addition to acting as a coreactant and providing radicals for the self-ECL of ZL-2, the introduction of the CO_3^{2-} ligand

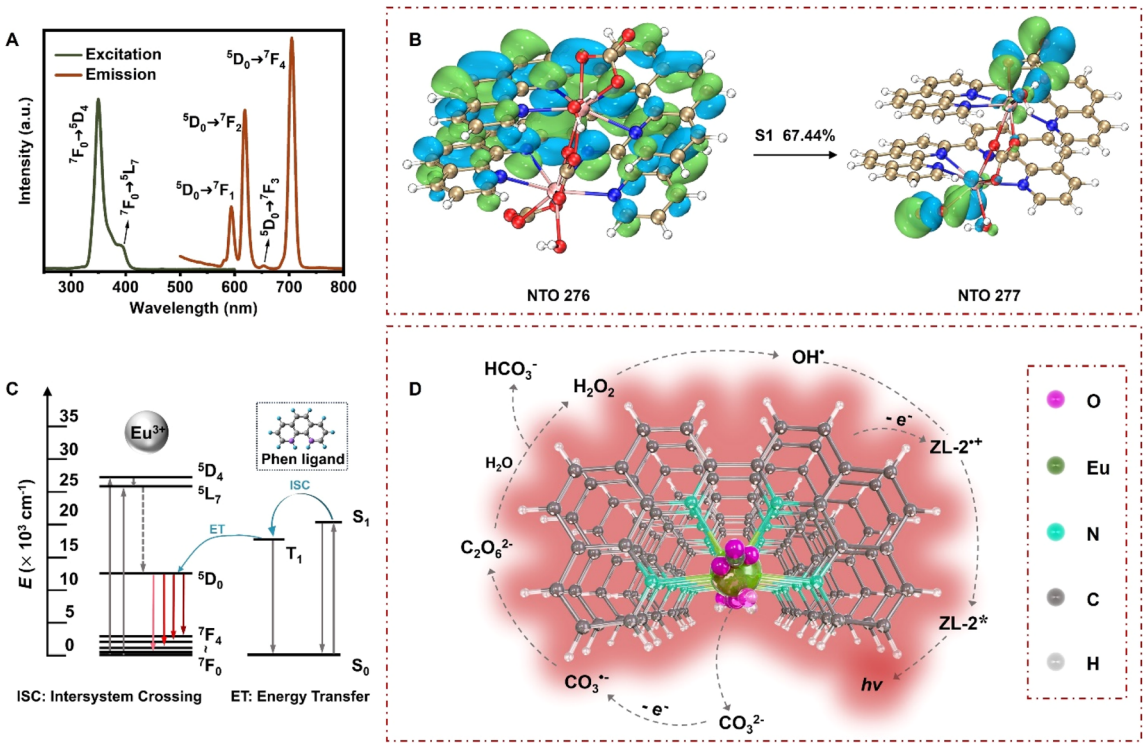

Fig. 3 (A) Excitation and emission spectra of ZL-2. (B) NTO isodensity surfaces of S_1 for ZL-2 clusters (isovalue = 0.02 a.u.; the numbers show the contributions of S_1 to the orbital). Green and blue regions represent the positive and negative orbital phases, respectively. (C) Simple model for the energy transfer processes of the Phen ligand to Eu^{3+} and the f–f transition emission mechanism of Eu^{3+} in ZL-2. (D) Schematic diagram of the deep-red self-electrochemiluminescence mechanism in ZL-2.

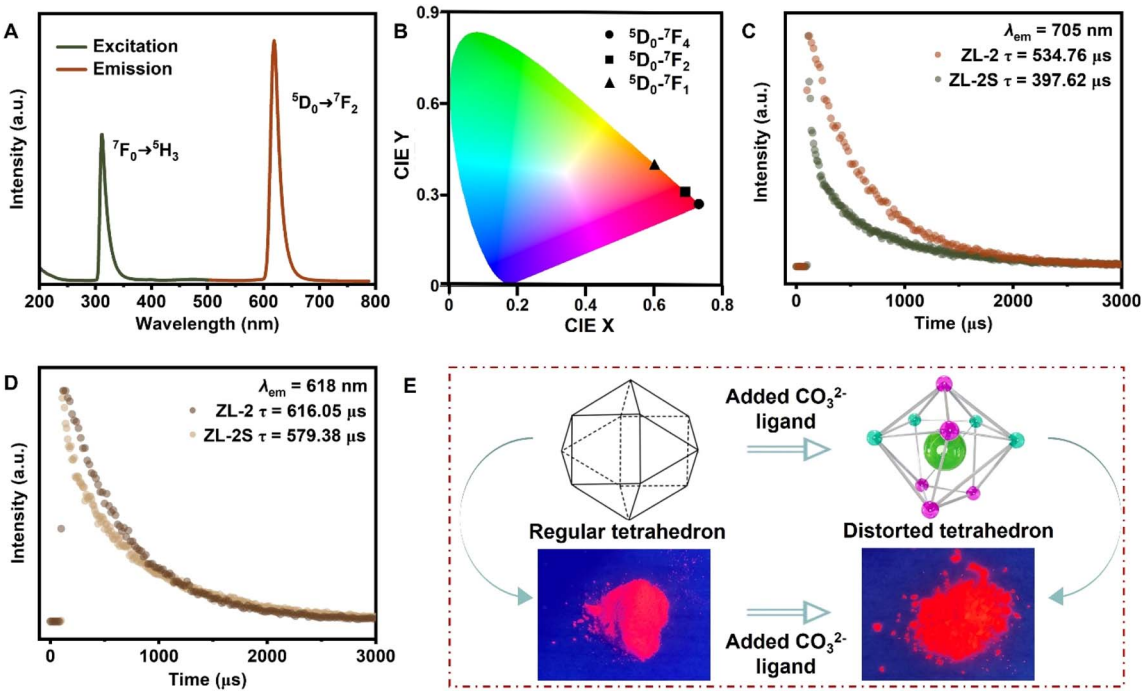

Fig. 4 (A) Excitation and emission spectra of ZL-2S. (B) CIE chromaticity diagram of $^5D_0-{}^7F_1$, $^5D_0-{}^7F_2$ and $^5D_0-{}^7F_4$ transitions in ZL-2. FL lifetimes for ZL-2 and ZL-2S under emission wavelengths of (C) 705 nm and (D) 618 nm. (E) Comparison of distorted tetrakaidecahedron structure of ZL-2 with the normal tetrakaidecahedron model, and corresponding luminescence photographs of ZL-2S and ZL-2 under a UV lamp (365 nm).

affected ZL-2 at the structural level, triggering ZL-2 to produce a rare deep-red luminescence. The emission peak of the $^5D_0-{}^7F_4$ transition at 705 nm for ZL-2 (Fig. 3A) was different from those of common europium-based materials, in which the strongest emission peak was attributable to the $^5D_0-{}^7F_2$ transition at 618 nm.[5] Similarly, the strongest emission peak of ZL-2S was also located at 618 nm, and even the peak at 705 nm was not observed (Fig. 4A), indicating that the presence of CO_3^{2-} induced in ZL-2 the ability for NIR luminescence. The luminescence intensity was enhanced after introducing CO_3^{2-}, besides the change in the dominant emission transition, which was discovered from a comparison of emission peak intensities (Fig. S9†) and the enhanced ECL signals in the presence of CO_3^{2-} (Fig. S6 and 7†). To investigate the effect of CO_3^{2-}, the fluorescence lifetimes of two major emission wavelengths at 618 and 705 nm for ZL-2 and ZL-2S were measured respectively (Fig. 4B–D). Compared to ZL-2S, the fluorescence lifetime of ZL-2 at 618 nm showed a slight increase from 579.38 μs to 616.05 μs. In particular, the lifetime at 705 nm was significantly improved from 397.62 μs to 534.76 μs. These phenomena brought about geometric distortion due to the addition of CO_3^{2-}.[5,28,29] The CO_3^{2-} ligand led to the substitution of Eu^{3+} to certain sites in the original tetrakaidecahedron structure (Fig. 4E). Therefore, the coordination polyhedron in ZL-2 presented a distorted square antiprism structure to trigger intense $^5D_0-{}^7F_4$ transition emission, inducing brighter deep-red luminescence, which could be observed under illumination by a UV lamp (365 nm) (Fig. 4E). The designed synthesis of the deep-red ZL-2 was a significant discovery for self-NIR-ECL applications.

Conclusions

An Eu-MOF featuring self-NIR-ECL emission was designed with Phen as the first ligand and CO_3^{2-} provided by Gly under strong alkaline conditions as the second ligand. Along with the antenna effect from the Phen ligand to the luminescence center Eu unit, the CO_3^{2-} ligand can provide an $OH^{\bullet}$ radical for the generation of excited Eu-MOF (ZL-2*) upon oxidation of CO_3^{2-} in an anodic ECL process. Meanwhile, the introduction of the CO_3^{2-} ligand twisted the tetrakaidecahedron structure of ZL-2 by inducing Eu^{3+} to occupy some sites, triggering the unusual electric-dipole transfer transition of $^5D_0-{}^7F_4$. Moreover, the cycle of the CO_3^{2-} ligand further enhanced the transition, leading to strong ECL emission in the deep-red region. This work extended the reported self-ECL emitters to the NIR field and broadened the function of the CO_3^{2-} ligand, which are beneficial to the development of self-ECL in related applications.

Data availability

All experimental procedures and ESI tables and figures are available in the ESI.† Crystallographic data for the structures reported in this paper are also deposited in the Cambridge Crystallographic Data Center with CCDC reference numbers 2427309 for the ZL-2.

Author contributions

L. Z. and X. S. designed the research, analyzed the data and wrote the manuscript. Z. X. carried out the experiments. C. D.

provided the funds. H. J. supervised the research and writing. All authors have participated in modification of the manuscript and given approval to the final manuscript.

Conflicts of interest

There are no conflicts to declare.

Acknowledgements

This study was supported by the National Natural Science Foundation of China (22404090 and 22374086), the Taishan Scholar Foundation of Shandong Province (tstp20231227), the Natural Science Foundation of Shandong Province (ZR2024QB064). All of authors express their sincere thanks.

Notes and references

1 Z. Ding, B. M. Quinn, S. K. Haram, L. E. Pell, B. A. Korgel and A. J. Bard, *Science*, 2002, **296**, 1293–1296.
2 X. Song, X. Ren, W. Zhao, L. Zhao, S. Wang, C. Luo, Y. Li and Q. Wei, *Anal. Chem.*, 2022, **94**, 12531–12537.
3 X. Song, L. Zhao, C. Luo, X. Ren, L. Yang and Q. Wei, *Anal. Chem.*, 2021, **93**, 9704–9710.
4 Y. Hong, W. Geng, T. Zhang, G. Gong, C. Li, C. Zheng, F. Liu, J. Qian, M. Chen and B. Tang, *Angew. Chem., Int. Ed.*, 2022, **61**, e202209590.
5 H. Zhang, Z. Yang, H. Li, J. Li, C. Liu, H. Jiang, Y. Liu, R. Wang, Z. Xie and J. Zhu, *Laser Photonics Rev.*, 2024, **18**, 2400463.
6 M. Hesari, M. S. Workentin and Z. Ding, *Chem. Sci.*, 2014, **5**, 3814–3822.
7 D. Zhu, Y. Zhang, S. Bao, N. Wang, S. Yu, R. Luo, J. Ma, H. Ju and J. Lei, *J. Am. Chem. Soc.*, 2021, **143**, 3049–3053.
8 X. Wang, S. Xiao, C. Yang, C. Hu, X. Wang, S. Zhen, C. Huang and Y. Li, *Anal. Chem.*, 2021, **93**, 14178–14186.
9 N. Wang, H. Gao, Y. Li, G. Li, W. Chen, Z. Jin, J. Lei, Q. Wei and H. Ju, *Angew. Chem., Int. Ed.*, 2021, **60**, 197–201.
10 L. Li, X. Hu, Z. Tang, C. Wang and H. Ju, *Anal. Chem.*, 2024, **96**, 4308–4313.
11 D. E. Barry, D. F. Caffrey and T. Gunnlaugsson, *Chem. Soc. Rev.*, 2016, **45**, 3244–3274.
12 D. Jiang, C. Huang, J. Zhu, P. Wang, Z. Liu and D. Fang, *Coord. Chem. Rev.*, 2021, **444**, 214064.
13 L. Zhao, X. Ren, Y. Du, Z. Gao, H. Ma, H. Wang, Y. Li, Q. Wei, H. Ju and D. Wu, *Adv. Funct. Mater.*, 2024, **34**, 2410886.
14 X. Meng, L. Zheng, R. Luo, W. Kong, Z. Xu, P. Dong, J. Ma and J. Lei, *Angew. Chem., Int. Ed.*, 2024, **63**, e202402373.
15 I. A. Fiorani, G. Valenti, N. Kamoshida, F. Paolucci and Y. Einaga, *J. Am. Chem. Soc.*, 2020, **142**, 1518–1525.
16 S. J. Wang, M. Wahiduzzaman, L. Davis, A. Tissot, W. Shepard, J. Marrot, C. Martineau-Corcos, D. Hamdane, G. Maurin, S. Devautour-Vinot and C. Serre, *Nat. Commun.*, 2018, **9**, 4937.
17 X. Wang, K. Gopalsamy, G. Clavier, G. Maurin, B. Ding, A. Tissot and C. Serre, *Chem. Sci.*, 2024, **15**, 6488–6499.
18 L. Zhao, X. Song, X. Ren, H. Wang, D. Fan, D. Wu and Q. Wei, *Biosens. Bioelectron.*, 2021, **191**, 113409.
19 L. Xia, F. Chen, J. Li, S. Chen, J. Bai, T. Zhou, L. Li, Q. Xu and B. Zhou, *J. Hazard. Mater.*, 2020, **389**, 122140.
20 Y. Wen, Y. Feng, J. Wei, T. Zhang, C. Cai, J. Sun, X. Qian and Y. Zhao, *Chem. Sci.*, 2024, **15**, 18969–18976.
21 W. Gu, L. Hu, W. Hong, X. Jia, J. Li and E. Wang, *Chem. Sci.*, 2016, **7**, 4167–4173.
22 X. Dou, Q. Zhang, S. N. A. Shah, M. Khan, K. Uchiyama and J. Lin, *Chem. Sci.*, 2019, **10**, 497–500.
23 S. T. Putnam and J. Rodríguez-López, *Chem. Sci.*, 2024, **15**, 10036–10045.
24 H. Zhu, X. Lv, Y. Wu, W. Wang, Y. Wu, S. Yan and Y. Chen, *Nat. Commun.*, 2024, **15**, 8846.
25 H. Wang, P. He, H. Yan and M. Gong, *Sens. Actuators, B*, 2011, **156**, 6–11.
26 L. Zhao, X. Song, X. Ren, D. Fan, Q. Wei and D. Wu, *Anal. Chem.*, 2021, **93**, 8613–8621.
27 W. Zhou, W. Lin, Y. Chen, X. Dai, Z. Liu and Y. Liu, *Chem. Sci.*, 2022, **13**, 573–579.
28 Z. Sun, J. Li, H. Qian, Y. Sakka, T. S. Suzuki and B. Lu, *J. Adv. Ceram.*, 2024, **13**, 113–123.
29 P. Hu, X. Guo, J. Hu, C. Deng and R. Cui, *Chem. Rev.*, 2024, **12**, 2301760.